Simulation of Mechanically Assembled Monolayers and Polymers in Good Solvent Using Discontinuous Molecular Dynamics

L. Anderson Strickland,* Carol K. Hall, and Jan Genzer

Department of Chemical & Biomolecular Engineering, North Carolina State University, Raleigh, North Carolina 27605-7905

Received February 12, 2008; Revised Manuscript Received June 10, 2008

ABSTRACT: We present the results of discontinuous molecular dynamics simulations of mechanically assembled monolayers in good solvent. Polymers of chain lengths 5−100 were end-grafted to surfaces at low density and then compressed laterally at varying rates. Data for brush thickness and end-monomer density were collected as a function of surface density; they were shown to correspond well with theoretical predictions and simulation results performed at constant surface density. Brush thickness for all chain lengths could be controlled by judicious choice of the compression rate. Defects in the brush layer were dependent on chain length; it was shown that quick compression for relatively short chains allowed the layer no time to relax into coil form. Quick compression on long chain systems led to entanglement in the brush layer since the longer-chained system was not being afforded the long relaxation time required to form a fully relaxed brush. Hysteresis effects were examined by allowing the brush to relax to a lower surface density, and it was shown that higher surface compression/relaxation rates led to an increase in disparity between brush thickness found during the compression and relaxation stages; in large part, this disparity was due to inadequate equilibration time. Last, results from nonuniform compression in good solvent show negligible effects on monolayer height and structure.

I. Introduction

Mechanically assembled monolayers (MAMs) are dense molecular assemblies formed by end-grafting oligomers onto a prestretched surface and then releasing the stretch, thereby increasing the surface density to levels higher than those typically found in systems composed solely of self-assembled monolayers (SAMs). Self-assembled monolayers are used in a variety of fields, including lubrication,[1] electrochemistry,[2,3] electronic and vibrational spectroscopy,[4,5] photochemistry,[4,6] electrical conduction,[4,7] catalysis,[8] and organic membranes.[9,10] Because of this wide array of uses, the ability to "tune" the surface characteristics of these monolayers is of vital importance. Although self-assembled monolayers allow for some adjustment of surface characteristics, their utility is limited due to the relatively low surface density of the grafting sites and the accompanying defects that allow penetration of liquids into the monolayer, especially polar liquids.

Mechanically assembled monolayers (MAMs) can rectify the problems associated with low grafting-site surface densities. By combining self-assembly with mechanical manipulation of the underlying substrate, researchers can create polymer layers or "brushes" which reach higher surface coverage than those achievable solely through self-assembly, thereby impeding or retarding surface degradation from liquid penetration. To this point, all of the research in the area of mechanically assembled monolayers has been experimental.[11−13] In their work, Genzer and Efimenko showed that mechanical stretching of a flexible substrate surface prior to tethering the oligomers or polymers through self-assembly would lead to the formation of dense, defect-free monolayers. Wu and co-workers subsequently extended the assembly of oligomers to surface-anchored polymers by introducing a "mechanically assisted polymer assembly" (MAPA).[14] Finally, Genzer, Fisher, and Efimenko demonstrated that the surface density of a polymer brush on a flexible substrate could be adjusted over a wide range due to the direct proportionality between initial strain in the substrate and final density of the brush.[15] The primary distinction between MAMs and MAPA is the length of the grafted chain. In order to simplify our discussion in this paper, we refer to both structures as MAMs.

The mechanism by which chains form highly packed MAMs is unclear. During the fabrication of MAMs, the surface strain is released, thereby increasing the surface density of the grafted molecules. As the layer shrinks, it densifies and becomes more ordered. The mechanism underlying this rearrangement process is unknown. It could be that a select polymer acts as a seed for nucleation around which other chains aggregate, generating an organized structure which then propagates throughout the entire surface. Alternatively, small localized groupings of a few molecules could form, which are then brought together mechanically as the stretch is released; organization of the entire layer would then occur on a global level. Also, the rate at which the surface is released and the quality of the solvent affect the thickness and ordering of the monolayer structure. Theory and previous experimental work can predict monolayer properties when the surface density is held constant. This work focuses on the densification which occurs in the MAMs formation process.

Surface-grafted polymers stretching in good solvent conditions were first studied by Alexander and de Gennes.[16,17] On the basis of the "blob" model,[18] Alexander put forth that the monomer segment density profile for a monolayer, $\rho(h)$, could be expressed as

$$\rho(h) = \rho_a^{(3\nu-1)2\nu} h^{(1-3\nu)(2-d)/2\nu} \quad (1)$$

where d is the dimensionality of the surface (2 for flat surfaces), h is the distance from the tether point, ρ_a is the surface density, and ν is the correlation length exponent for isolated chains in good solvents, which is approximately 0.6 (refer to ref 19, eq 9.1). For $d = 2$, the density is independent of the distance from the surface. Scaling theory states that the brush height h_{max}, defined as the thickness of the layer over which the brush density is constant, scales as

$$h_{max} \sim N\rho_a^{1/3} \quad (2)$$

where N is the chain length of the polymer, provided that ρ_a is above the critical overlap density, $\rho^*_a \sim N^{-6/5}$. Below ρ^*_a, h_{max}

* To whom correspondence should be addressed.

10.1021/ma8003218 CCC: $40.75
Published on Web 08/05/2008

is nearly independent of surface density. Equation 2 reveals that the height of a two-dimensional monolayer ($d = 2$) depends linearly on the length of the chain.

The work of Alexander and de Gennes was expanded upon by Skvortsov et al.,[20] Milner et al.,[21,22] and Zhulina et al.[23] Milner used numerical self-consistent-field (SCF) theory to show that the density profile for a monolayer of long chains in high concentration "flattens". For low concentration of chains, the density profile is instead parabolic. Zhulina et al. used analytical SCF to show that the density profile, $\rho(h)$, in low concentration could be expressed as

$$\rho(h) = C_1\rho_a^{2/3} - C_2(h/N)^2 \tag{3}$$

where C_1 and C_2 are spatial-constraint constants and h is the height above the surface, provided monomer−monomer interactions are binary. Numerous simulations and experimental studies have validated the parabolic density profile model for tethered polymers.[24–27] Similarly, it was shown that the density profile for tethered polymer tail groups [$\rho_E(h)$] for moderate density brushes (eq 4) and for more dense brushes (eq 5) is given by

$$\rho_E(h) = C_3\rho_a^{-2/3}N^{-2}h[1 - (h/h_{max})^2]^{1/2} \tag{4}$$

$$\rho_E(h) = C_4\rho_a^{-2/3}N^{-2}h[1 - (h/h_{max})^2]^{-1/2} \tag{5}$$

where h_{max} is the maximum brush height and thickness at which the density vanishes.[19,28] Because of the $-1/2$ exponential power for the more dense brush, eq 5 diverges at $h \sim h_{max}$, meaning most of the polymer ends are far from the wall. It should also be noted that according to eqs 4 and 5 $\rho_E(h)$ is implicitly nonzero for all h greater than zero. Thus, tail groups are not restricted to inhabiting only the outer reaches of the tethered film but are also allowed to explore space near the tethering surface.

In this paper, we present the results of discontinuous molecular dynamics simulations of the compression of systems of polymers modeled as hard chains in an attempt to mimic the MAMs formation process. Polymers of chain lengths ranging from 5 to 100 were initially grafted to a surface at low density (typically, below 0.200 monomers/area) and allowed to equilibrate. These layers were then compressed at varying rates to high surface density to study the effects of chain length and compression rate on monolayer formation; by compressing at frequencies larger than the brush's equilibrium time scale, we could assess how brush thickness and structure are affected during the MAM formation process. Next, select systems were decompressed to the initial surface density to study hysteresis effects. Finally, monolayers were compressed disproportionally in one direction to investigate the effects of nonuniform compression on ordering.

Highlights of this work are as follows. Data presented show that regardless of compression rate monomer density profiles for the monolayer fit theoretical predictions and previous experimental work to a close approximation. We show that throughout the MAMs formation the monolayer thickness consistently scales as $N\rho_a^{1/3}$, in accordance with the theory of Alexander and DeGennes. We see that compression allows for high surface densities which would be difficult to attain solely through self-assembly and that this high surface coverage and compression engenders quasi-crystalline formation near the surface and "encourages" end monomers to move away from the surface. Last, when monolayers are allowed to relax to the original surface density or nonuniform compression is applied, the effect on layer formation is negligible.

The remainder of the paper is organized as follows. In section II, we discuss the discontinuous molecular dynamics method and our process for compressing the surface. Section III presents the simulation results for various chain lengths N and various compression rates and modes. In section IV, we compare these results with theoretical predictions and previous simulations. Section V concludes with a short summary of the results and a discussion.

II. Model and Method

We simulate the formation of a mechanically assembled monolayer by using the discontinuous molecular dynamics (DMD) method. Traditional molecular dynamics employs a monomer−monomer interaction potential that is a continuous function of their separation (i.e., the Lennard-Jones potential), which incorporates short-range repulsions as well as long-range attractions. The trajectories of a system of monomers are repeatedly advanced at a small increment in time, after which the forces between all pairs of monomers are reevaluated. DMD, on the other hand, replaces the continuous potential function with a discontinuous function, such as a hard-sphere repulsion or square-well attraction. At long range, monomers feel no attraction.[29] In this work, we are concerned only with short-ranged excluded volume effects. As the monomers feel only volume exclusion and no long-range attraction to one another, this implies good solvent conditions. The potential energy for nonbonded monomer−monomer interactions at distance r is given by the hard-sphere potential

$$\begin{aligned} U(r) &= \infty, \quad r \le \sigma \\ &= 0, \quad r > \sigma \end{aligned} \tag{6}$$

where σ is the monomer diameter.

The advantage of using DMD over traditional MD is that the monomers do not need to be moved at short regularly spaced time steps as in traditional molecular dynamics. Instead, one only needs to calculate the time until the next collision for each monomer, t_{ij}, and the monomer's new postcollision velocity.[30,31] The collision time between monomer i and all monomers $j \neq i$ is given by

$$t_{ij} = \frac{-b_{ij} \pm \sqrt{b_{ij}^2 - v_{ij}^2(r_{ij}^2 - \sigma^2)}}{v_{ij}^2} \tag{7}$$

where $\mathbf{r}_{ij} \equiv \mathbf{r}_i - \mathbf{r}_j$ is their relative position, $\mathbf{v}_{ij} \equiv \mathbf{v}_i - \mathbf{v}_j$ is their relative velocity, and $\mathbf{b}_{ij} \equiv \mathbf{r}_{ij} \cdot \mathbf{v}_{ij}$.[32] Next, the minimum collision time for the system, t_c, is chosen and all monomers are moved according to

$$\mathbf{r}_i(t + t_c) = \mathbf{r}_i(t) + \mathbf{v}_i(t_c) \tag{8}$$

where $\mathbf{r_i}$ and $\mathbf{v_i}$ represent the ith monomer's position and velocity, respectively. At this point, exactly two monomers collide while the remainder of the monomers are separated from one another. New velocities for the colliding monomers are calculated using conservation of momentum and conservation of kinetic energy.

Systems of polymers can be modeled as freely jointed chains of monomers bonded at distance σ from one another. When one monomer undergoes a collision, the effect is felt instantaneously by those monomers to which it is bonded. Since bonded monomers are constantly attempting to deviate from the prescribed σ distance, these deviations can be computationally expensive. To decouple the motions of neighboring monomers, Rapaport developed an algorithm which allows the bond length to vary freely over the range σ to $\sigma(1 + \delta)$, where δ is very small.[33,34] Thus, two bonded monomers move freely without interacting when their separation is between σ and $\sigma(1 + \delta)$; however, they undergo a hard-sphere repulsion when $r = \sigma$ or $r = \sigma(1 + \delta)$. Bellemans et al. applied one further modification (which is employed in this work). They allowed the bonded monomers to fluctuate over a range $\sigma(1 \pm \delta)$.[35] In this case, the average bond length is σ and thus closer in architecture to chains constructed of tangentially connected monomers.

The temperature of the system and, concordantly, the total kinetic energy are held constant throughout the simulation. To regulate temperature, we employ a heat bath in the form of an Andersen thermostat,[36] which allows the temperature to fluctuate about an average system temperature, $T^* \equiv k_B T/\varepsilon$. This is accomplished by having monomers (nontether points) collide stochastically with "ghost" particles, which then change the monomers' velocity. After particle i collides with a "ghost particle", new collision times must be calculated for this particle and for all other particles j which, prior to the ghost collision, would have collided with i. The time between ghost collisions, t_g, is random and is calculated by

$$t_g = A|\cos(2\pi R)\sqrt{(-2\log(R))}| \tag{9}$$

where R is a random number between 0 and 1 and A is a coefficient which controls the frequency with which the ghost collisions occur; A must be manipulated for each system so that the fluctuations in T are neither too big nor too small.

We model the monolayer as a system of M chains tethered to a flat surface; each chain contains N hard-sphere monomers and is freely jointed. All intermediate monomers are bound to two neighbors at a distance $\sigma(1 \pm \delta)$, where $\delta = 0.10$. This model is sometimes referred to as the hard-chain or pearl-necklace model.[37] Each chain or polymer is grafted at one end ($z = 0$) to a surface of area S. The tether point for each chain is initially assigned velocities in the x- and y-directions and allowed to wander along (but not detach from) the surface. The surface density, ρ_a, is $\rho_a = M/S$. Monomers are allowed to move freely such that the bond angle along the chain can assume any value as long as there is no monomer−monomer overlap. This model incorporates two major features of a polymer molecule: connectivity and excluded volume.

Grafting the polymers to a surface introduces two additional considerations: monomer collisions with the surface and tether point collisions. For all monomers except those directly connected to the surface, the collision time between any monomer i and the surface is calculated by

$$t_i = \mathbf{r}_{iz}/|\mathbf{v}_{iz}| \tag{10}$$

where $\mathbf{r}_{iz}$ and $\mathbf{v}_{iz}$ are monomer i's position and velocity in the z-direction, respectively. (Here, the absolute value of velocity in the z-direction is required since our system is set up with the z-axis pointing away from the surface.) Conversely, we allow the monomer connected to the grafting surface to fluctuate over distance $\sigma(1 \pm \delta)$ from the hard surface. The collision time between a grafted monomer and the surface is calculated similarly to that between bonded monomers. Also, collision times for the tether point for each chain must be calculated. Since these points cannot move from the surface, we need only to calculate the hard-sphere collision time for each tether point with other tether points in the x- and y-directions to ensure no overlap of the chains at the surface. (We do this so that, similar to experimental work, each chain is bound to a unique position on the surface.)

Periodic boundary conditions for the simulation box, which is of length L_x and width L_y, are used in the x- and y-directions. Periodic boundary conditions are not used in the z-direction since monomers are bound as chains grafted to the surface and, thus, cannot escape in the z-direction. (There is no hard ceiling in the z-direction as box pressure is of no interest in this work.)

The release of previously stretched monolayers is modeled by attempts to compress the surface at uniformly spaced intervals. At prescribed collision numbers (say, every 500th collision), new box dimensions are calculated:

$$L_x(\text{new}) = L_x(\text{old})\left(1 - \delta_{L_x}\right) \tag{11}$$

$$L_y(\text{new}) = L_y(\text{old})\left(1 - \delta_{L_y}\right) \tag{12}$$

where δ_{L_x} and δ_{L_y} are very small (on the order of 1×10^{-5}) compared with L_x and L_y (on the order of 10−50 times σ). Typically, δ_{L_x} and δ_{L_y} are identical to describe equal compression in the x- and y-directions, but their ratio can be adjusted. New monomer positions are calculated:

$$\mathbf{r}_{jx}(\text{new}) = \mathbf{r}_{jx}(\text{old})\left(1 - \delta_{L_x}\right) \tag{13}$$

$$\mathbf{r}_{jy}(\text{new}) = \mathbf{r}_{jy}(\text{old})\left(1 - \delta_{L_y}\right) \tag{14}$$

where $\mathbf{r}_i$ is the position of monomer i. If the new positions of all particles do not violate any excluded volume constraints or any bonded-monomer chain length constraints, the new positions are accepted. The new surface density and new surface area, $\rho_a = M/(L_{x,\text{new}}L_{y,\text{new}})$ and $S = L_{x,\text{new}}L_{y,\text{new}}$, respectively, are calculated. If there is a violation of constraints, the old positions and box dimensions are retained. For the purpose of this paper, the relaxation rate of the surface will be defined to be the frequency at which these compression attempts are performed; this will differ from the actual success rate of the compression.

After each compression move, data are collected for the polymer layer's mean-square radius of gyration, $\langle R_g^2 \rangle$, and the mean-square radius of gyration in the z-direction, $\langle R_{g,z}^2 \rangle$, which are defined respectively as

$$\left\langle R_g^{\,2} \right\rangle = 1/N\left\langle \sum (\mathbf{r}_i - \mathbf{r}_{CM})^2 \right\rangle \tag{15}$$

$$\left\langle R_{g,z}^{\,2} \right\rangle = 1/N\left\langle \sum (\mathbf{r}_{zi} - \mathbf{r}_{z,CM})^2 \right\rangle \tag{16}$$

where $\mathbf{r}_{zi}$ is the z-coordinate of the ith monomer position ($\mathbf{r}_i$) and $\mathbf{r}_{z,CM}$ is the z-coordinate of the center of mass for the corresponding chain's center of mass, $\mathbf{r}_{CM}$; the summation is taken over all monomers N along each chain and then averaged for each chain in the system. Over the course of the monolayer compression, we also collected monomer density profiles, $\rho(z)$, and density profiles for the free ends, $\rho_E(z)$. (These data are normalized such that $\int \rho(z)\, dz = 1$ for all systems.)

We simulate the compression and relaxation of systems containing $M = 25$ and $M = 50$ grafted polymers of chain lengths $N = 5$, 10, 20, 50, and 100 at initial surface densities of $\rho_a = M/S$ ranging from 0.01 to 0.20. The systems that we study are shown below in Table 1, along with values of $\langle R_{g,z} \rangle^2$ and $\langle R_g \rangle^2$ which are found during simulation. An initial temperature, $T^* = 1.20$, is chosen and initial velocities are assigned according to a Gaussian distribution to the monomers of diameter $\sigma = 1.0$. After the systems are equilibrated at the initial surface density, compression moves (typically, every 500th, 2000th, or 10000th collision) are attempted and, if allowed, also applied. Between compressions, standard discon-

Table 1. Mean-Squared z-Directional Radius of Gyration, $\langle R_{g,z} \rangle^2$, and Radius of Gyration, $\langle R_g \rangle^2$, for M Chains of N Length at Surface Density, ρ_a[a]

M	N	ρ_a	$\langle R_{g,z} \rangle^2$	$\langle R_g \rangle^2$
50	5	0.01	0.45	1.0
50	5	0.03	0.41	1.0
50	5	0.1	0.47	1.1
50	10	0.1	1.55	3.4
50	20	0.01	2.67	7.8
50	20	0.03	3.01	7.6
50	20	0.1	5.26	8.7
50	50	0.01	10.36	24.8
50	50	0.03	13.60	25.1
50	50	0.1	29.69	38.5
50	50	0.2	49.76	55.0
25	100	0.03	55.81	81.2

[a] Simulations were performedat reduced temperature, $T^* = 1.20$.

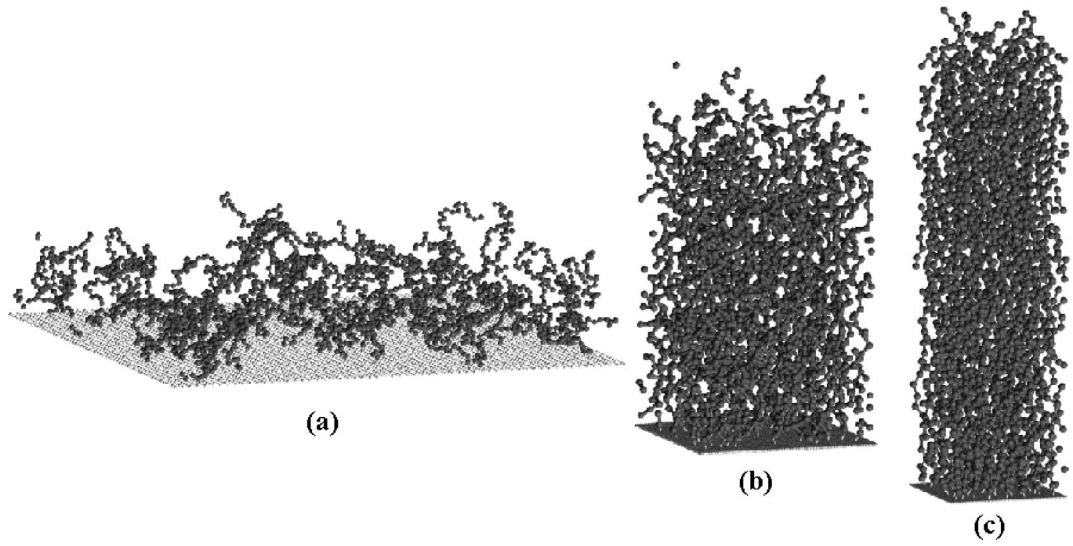

Figure 1. (a) A system consisting of 50 polymers of 50 monomers each at an initial surface density of 0.01monomers per area is compressed every 500th collision to (b) surface density 0.200 and (c) finally to 0.500.

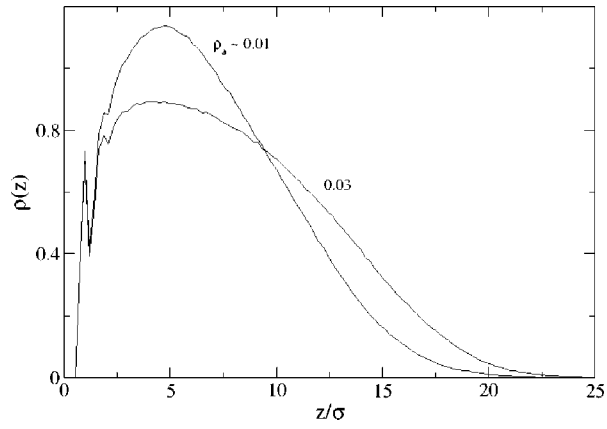

Figure 2. Monomer density profile, $\rho(z)$, as a function of distance from the surface, z, for a system of 50 50-mers compressed from initial surface density $\rho_a = 0.01$ to final surface density $\rho_a = 0.03$.

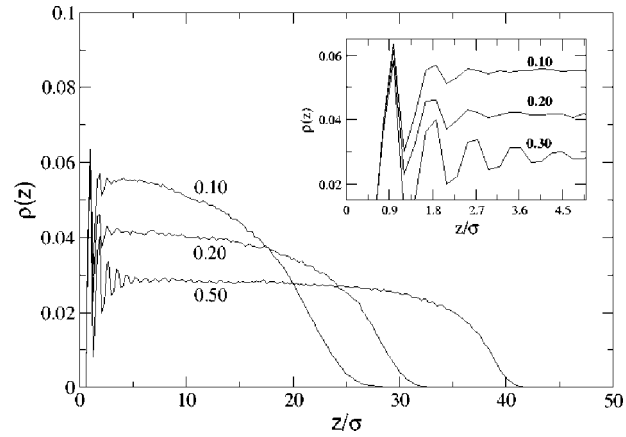

Figure 3. Monomer density profile, $\rho(z)$, as a function of distance from the surface, z. The system from Figure 2 has been further compressed to (a) $\rho_a = 0.10$, (b) $\rho_a = 0.20$, and finally to (c) $\rho_a = 0.50$. Inset magnifies region near surface.

tinuous molecular dynamics moves are used, and collision times are calculated according to the rules laid out above. In general, this process increases the surface density to 0.500 monomers per area or higher. Results for these simulations are described in detail in the following section.

III. Results

Snapshots of a system of 50 polymers composed of 50 monomers are shown in Figure 1 as it is compressed from (a) $\rho_a = 0.01$ to (b) 0.20 to (c) 0.500. We see in Figure 1b that compression to surface density $\rho_a = 0.20$ overcomes one of the drawbacks of self-assembled systems: monolayer openings. Further compression to $\rho_a = 0.50$ thickens the monolayer and encourages movement of the polymer ends outward from the surface. These trends were followed for all systems, especially for chain lengths over $N = 20$.

The monomer density profiles for a system of 50 50-mers at surface densities 0.01 and 0.03 are shown in Figure 2. We note first that the density profile at surface density $\rho_a = 0.01$ shows two peaks: a very sharp peak (local maximum) near 1σ corresponding to the monomers from each chain directly grafted to the surface and a broader peak near 5σ corresponding to the average z-coordinate values for the monomers. We note that low surface coverage encourages the chains to remain near the surface at distances 1/5th to 1/10th of their chain length rather than to extend their conformation; we conclude that at this low surface coverage there is relatively little chain−chain interaction. Figure 2 also depicts the density profile for the same system compressed to surface area 0.03. While the density profile retains the sharp peak near 1σ (the grafted monomers have little freedom to fluctuate), we detect an overall flattening of the profile and a general shift to the right toward higher z-values as the polymer chains straighten due to volume exclusion effects.

Further compression to higher surface coverage serves to increase the volume exclusion effect. Since the chains feel no attraction to each other, reduction of space in the x- and y-directions forces them to move away from the surface, allowing them to explore the relatively limitless space in the z-direction. Figure 3 presents the monomer density profile for the system of 50 50-mers shown in Figure 2 after it has been compressed to surface densities of $\rho_a = 0.10$, $\rho_a = 0.20$, and finally to $\rho_a = 0.50$. There are two observations of note. First, at the highest surface density of $\rho_a = 0.50$, the density profile is nearly flat over most of the range, with a drop-off far from the surface. From this, we infer that the chains are essentially stretching straight out from the surface. Additional evidence for this is the snapshot shown in Figure 1c. Second, the density profile oscillates near the surface. As the chains are forced to stretch out from the surface due to the high grafting density,

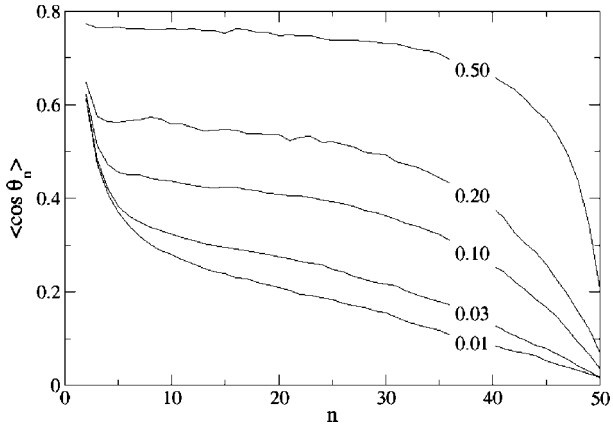

Figure 4. Orientation order parameter $\langle \cos \theta_n \rangle$ as a function of monomer number along the chain, n, for surface densities $\rho_a = 0.01$, $\rho_a = 0.03$, $\rho_a = 0.10$, $\rho_a = 0.20$, and $\rho_a = 0.50$.

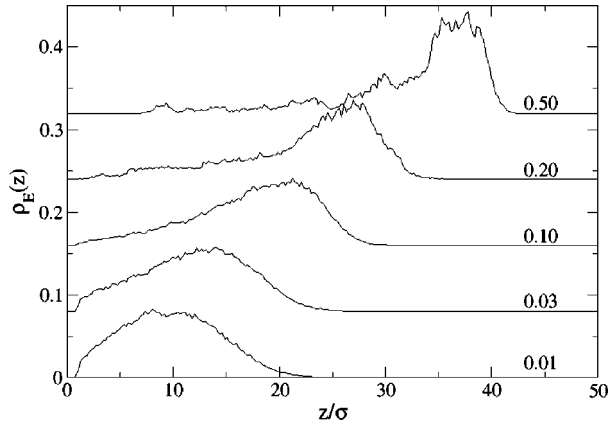

Figure 5. End-monomer density profile, $\rho_E(z)$, as a function of distance from the surface, z, at surface densities $\rho_a = 0.01$, 0.03, 0.10, 0.20, and 0.50. Each graph has been shifted vertically 0.08 relative to the preceding graph for clarity.

the monomers near the surface occupy positions in the z-direction that are discrete multiples of $\sigma(1 - \delta)$. As can be seen in the inset of Figure 3, the high surface density seems to engender order (in the z-direction) near the surface. The ordering of the layer begins at the surface and then progresses outward as the monolayer is compressed to higher surface density. However, the ordering is not truly crystalline; when viewing a top-down projection of the monomers directly attached to the surface, there is no ordering in the x- or y-direction. Thus, while there is some ordering in the z-direction due to the stretching of the chains, this is purely the result of a loss of conformational options. No ordering has propagated laterally.

As the surface density increases due to compression, the chains align with one another. Polymer stretching and ordering are depicted in Figure 4, which shows the orientational order parameter, $\langle \cos \theta_n \rangle$ as a function of monomer number along the chain, n, for various surface densities. Here, $\cos \theta_n$ is defined as

$$\cos \theta_n = (z_n - z_{n-1})/|\mathbf{r}_n - \mathbf{r}_{n-1}| \tag{17}$$

where $n = 0$ at the surface and θ_n is defined as the angle between the bond formed by successive monomers in the chain and the z-axis. Increasing the surface density from $\rho_a = 0.01$ to $\rho_a = 0.50$, we see that for high surface densities the orientational order parameter is nearly constant (around 0.75) for most of the chain length. Hence, the majority of the chain's monomers are stretched out from the surface. As these data take into account all chains in the system, we can infer that the nth monomer is at nearly the same distance from the wall for each chain; this vertical organization is backed up by the sharp peaks in the inset of Figure 3. This compactness, along with the high surface density, creates an effective barrier; the chains' close proximity to one another prevents the appearance of permeable voids in the monolayer. A chain's ability to effectively influence the conformation of its neighbors is a direct function of its ability to stretch.

While a thick, well-organized monolayer is certainly critical in forming an impermeable brush, of equal importance is the location of the end monomers. Since end-monomer units would likely be tailored to interact with a contacting fluid, it is important that the end monomers be near the layer surface (furthest from the grafting surface). We studied how surface compression affects the location of the end monomers. Figure 5 depicts the end-monomer profile, $\rho_E(z)$, for a system of 50-mers. Initially, the system of chains is grafted at a surface density of $\rho_a = 0.01$ monomers/area. Since there is little chain−chain interaction, the end monomers are free to explore any location above $z = \sigma$ (due to wall repulsion). Compression of the surface

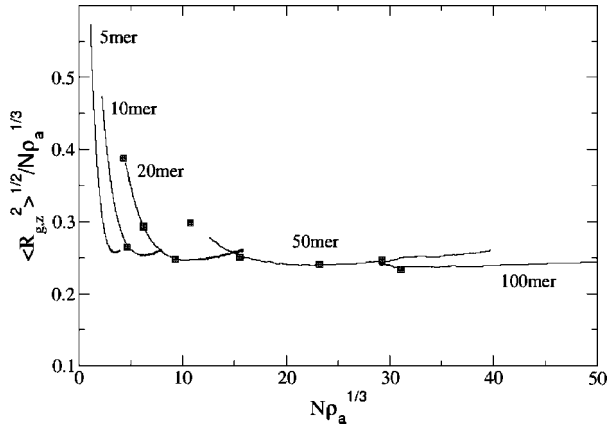

Figure 6. Normalized radius of gyration in the z-direction as a function of $N\rho_a^{1/3}$ for 5-mers, 10-mers, 20-mers, 50-mers, and 100-mers. Also shown is the equilibrium data (■) from Murat and Grest data.[38]

results in two trends: first, the end monomers naturally move away from the wall (although, $\rho_E(z)$ is still nonzero for values z near the wall), and second, the general shape of $\rho_E(z)$ shifts from parabolic at low densities (say, below $\rho_a = 0.1$) to a more sharply defined peak at high densities (say, $\rho_a = 0.50$). As the surface density increases, the end monomers move from the interior of the monolayer to the outer edge.

As stated previously in section I, Alexander and de Gennes used a "blob model" to postulate that the brush thickness of a two-dimensionally tethered surface would scale as $N\rho_a^{1/3}$, where N is the polymer chain length and ρ_a is grafting density. Previous molecular dynamics work done in this field showed that this theory held true for systems which were equilibrated over long periods of time at a specific surface density.[38] One aim of this work was to see whether rapid compression of the surface causes any deviation from scaling theory. Accordingly, we show in Figure 6 the radius of gyration in the z-direction normalized by $N\rho_a^{1/3}$ as a function of $N\rho_a^{1/3}$ for systems of chains which were not allowed to equilibrate during compression. For comparison, we also show data collected by Murat and Grest using molecular dynamics for systems of brushes which were allowed to equilibrate at fixed surface density. (Simulation data on off-lattice and lattice models of polymer brushes have also been presented by Carignano and Szleifer.[39,40]) Systems were initially at low surface density (typically 0.01 monomers/area). $\langle R_{g,z} \rangle^2$ values were collected continually as the surface was compressed using a compression rate of 1 attempt per 2000 collisions. In the regime where scaling theory is applicable, $\langle R_{g,z} \rangle^2$ normalized

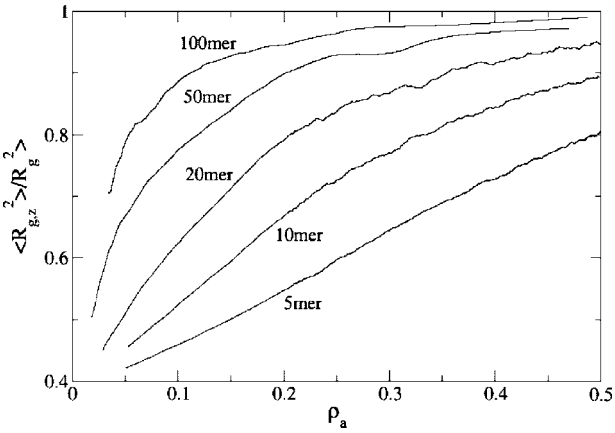

Figure 7. Ratio of the radius of gyration in the z-direction to the overall radius of gyration for 5-mers, 10-mers, 20-mers, 50-mers, and 100-mers as a function of surface density.

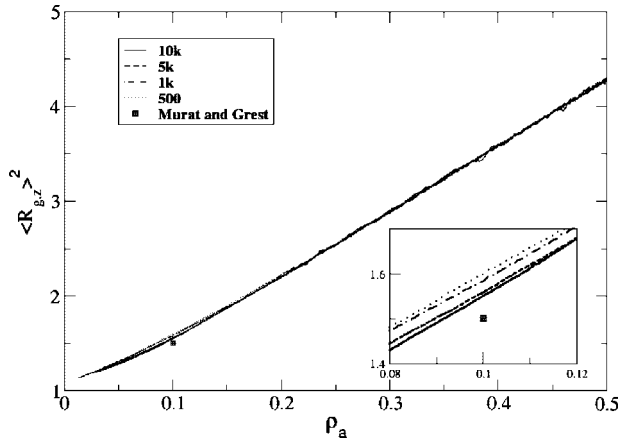

Figure 8. Mean-square radius of gyration in the z-direction as a function of surface density for a system of 10-mers compressed at rates of 500, 1000, 5000, and 10000 collisions per compression attempt. Also shown are equilibrium data from Murat and Grest.[38]

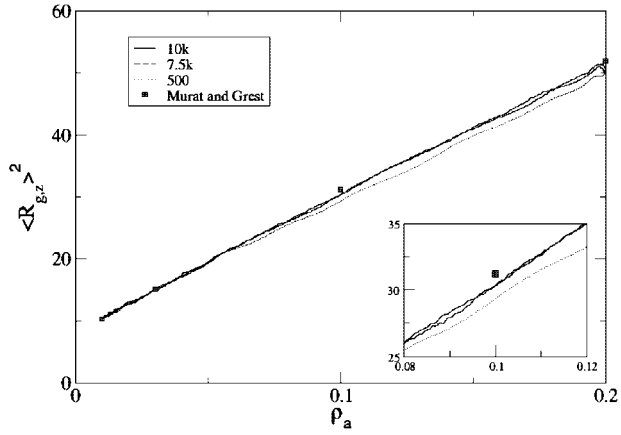

Figure 9. Mean-square radius of gyration in the z-direction as a function of surface density for a system of 50-mers compressed at rates of 500, 7500, and 10000 collisions per compression attempt. Also shown are equilibrium data from Murat and Grest.[38]

by $N\rho_a^{1/3}$ should be constant as a function of $N\rho_a^{1/3}$ (horizontal line). On the other hand, we note that for short chain lengths (5-mer and 10-mer), scaling theory works only for brushes which have been compressed beyond a moderate surface density of 0.2 monomers/area (or $N\rho_a^{1/3} \sim 3$ and 6, respectively). By comparison, longer chains (50-mer and 100-mer) fit scaling theory for nearly all surface densities throughout compression, primarily due to their large value of N. We can infer that individual chains of the longer-chained brushes begin to interact at a lower surface density than the short-chained systems.

Since one advantage of using a long polymer in a brush is that it reduces the need for high surface densities, this also reduces the required amount of initial mechanical stretching of the substrate. In Figure 7, we plot $\langle R_{g,z}\rangle^2/\langle R_g\rangle^2$, a measure of the extension of the chains in the brush, vs surface density. Note that to develop a highly extended brush where $\langle R_{g,z}\rangle^2/\langle R_g\rangle^2$ is say 95%, one needs only a surface density of 0.2−0.3 monomers/area for chain lengths $N \geq 50$. To reach that same proportionality though with shorter chains (e.g., $N = 20$), a surface area greater than 0.500 monomers/area is required; for example, 5-mers would require $\rho_a = 1$ (idealistic and in practice wasteful). Obviously, relatively long chain lengths are in one's best interest when producing MAMs.

Data for the results in the preceding paragraphs were collected from systems where the compression rates were relatively low, a compression attempt every 2000th collision. There is time for the brush to reorganize somewhat but not to completely equilibrate. To investigate the effects of compression rates on the mean-square radius of gyration in the z-direction, $\langle R_{g,z}\rangle^2$, a rough measure of the monolayer thickness, we attempted compression moves every 10000th, 5000th, 1000th, or 500th collision. Varying the compression rate has little effect on brush thickness for 5-mers; the equilibration time for a brush composed of 5-mers is low enough that the compression rate does not affect brush thickness. Figure 8 shows $\langle R_{g,z}\rangle^2$ vs surface density for 10-mers; data from Murat and Grest (equilibrium data) are also shown. In general, data from the four compression rates are nearly identical; there is little dependence on the compression rate. The inset to Figure 8 zooms in on the region surrounding $\rho_a = 0.1$. We note that the faster the surface compression, the higher the value of $\langle R_{g,z}\rangle^2$ (and, correspondingly, the larger the difference in value from Murat and Grest's equilibrium data). The faster compression rates do not afford the layer time to equilibrate. We can measure the relative amount of equilibration time for each system by determining the number of collisions each monomer undergoes on average between compression attempts, calculated as [shrink rate/number of chains/(chain length + 1)]. Thus, in cases of very small systems such as 50 10-mers, compression attempts every 10000th collision allow each monomer to undergo 10000/50/11 or ∼18 collisions between attempt; this is significant, allowing for steady chain and brush equilibration during compression. Faster compression rates though test the layer's ability to reorganize. The same system of 50 10-mers compressed every 500th collision averages about 0.91 collisions per monomer between collision attempts; the chains do not have a chance to relax. Therefore, experimenters must give attention to MAM formation rates, as increasing surface density too quickly leads to monolayer buckling and/or chain detachment from the surface.

While brush thickness during compression of short-chained systems tended to be higher than that of previously published simulation results, brush thickness during compression of longer-chained systems exhibited opposite tendency. In Figure 9, we show $\langle R_{g,z}\rangle^2$ vs surface density for 50-mers. We see a similar trend as before, wherein $\langle R_{g,z}\rangle^2$ data for the slower rates (10K and 7.5K) are more comparable to equilibrium data than fast compression. Unlike the 10-mers though, the $\langle R_{g,z}\rangle^2$ data for 50-mers lies under the equilibrium data of Murat and Grest. Most likely, the long chains are having trouble stretching through the highly dense, thick layer to achieve the equilibrated brush height; i.e., the relaxation time for 50-mers is larger than the frequency of our compression, and the result is a reduction in brush thickness.

It is posited by Genzer and co-workers that one advantage of MAMs over self-assembled monolayers is that the surface

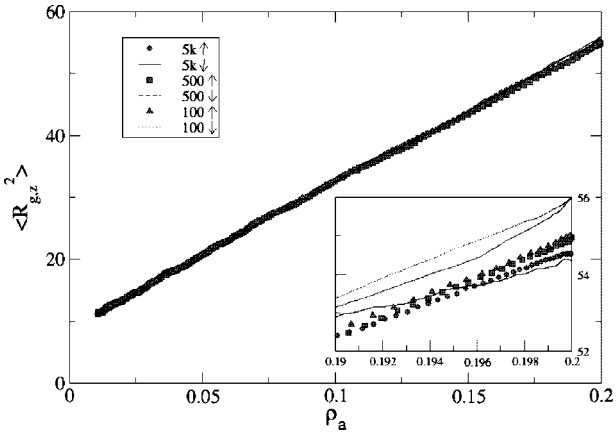

Figure 10. Plot of hysteresis in $\langle R_{g,z} \rangle^2$ vs surface density for compression rates 100, 500, and 5000 collisions per compression attempt. Compression values are shown as symbols and relaxation values are plotted as lines.

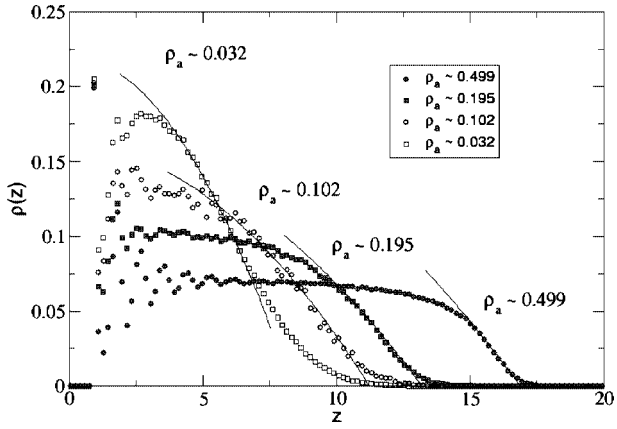

Figure 11. Density profile $\rho(z)$ vs z showing C_1/C_2 fit of eq 19 for 20-mers at various values of ρ_a.

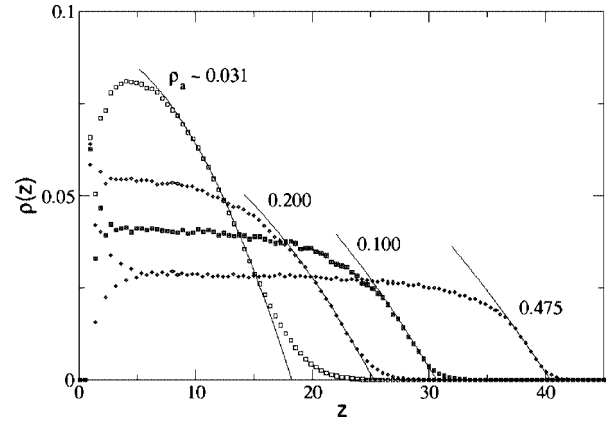

Figure 12. Density profile $\rho(z)$ vs z showing C_1/C_2 fit of eq 19 for 50-mers at various values of ρ_a.

density is not permanent; MAMs can be restretched to a lower surface density. One drawback to restretching would be possible adverse effects on brush formation and brush height. Accordingly, in our work, we compressed systems of grafted polymers to a high surface density ($\rho_a = 0.200$ monomers/area), equilibrated for several million collisions and then decompressed the system back to the initial density by stretching the surface at the same rate as in the previous compression. This created hysteresis loops that depend on the different compression/stretch rates. Figure 10 shows $\langle R_{g,z} \rangle^2$ vs surface density for three compression/stretch rates: a compression or stretch attempt every 100th, 500th or 5000th collision. It is noted that during the compression phase (symbols ◆, ■, and ▲) $\langle R_{g,z} \rangle^2$ values for all three cases are roughly equal. As found earlier, varying compression rate resulted in negligible difference in monolayer thickness. The inset of Figure 10 depicts $\langle R_{g,z} \rangle^2$ values near $\rho_a = 0.200$ for compression (symbols) and stretch (lines) modes. The $\langle R_{g,z} \rangle^2$ values for the slowest stretch rate (every 5000th collisions) correspond well with the values during compression. In contrast, the $\langle R_{g,z} \rangle^2$ values for the fastest stretch (every 100th collision) do not match their corresponding compression data; at any value of ρ_a, brush height during stretching is 1%−2% higher than during compression.

A final area of investigation is the effect of nonuniform compression on brush formation. Experimentally, Genzer and co-workers formed MAMs by mechanically manipulating the substrate in one direction only (call it Δx). Thus, upon release of the stretch, grafted monomers would feel a force of compression in only the x-direction. In contrast, simulation data shown up to this point was for systems compressed equally in the x- and y-directions. To test nonuniform compression, we define a nonuniformity parameter K as

$$K = (L_{x,\text{old}} - L_{x,\text{new}})/(L_{y,\text{old}} - L_{y,\text{new}}) \tag{18}$$

where L_x and L_y are the lengths of the simulation surface in the x- and y-directions, respectively. Here, "old" and "new" represent dimensions before and after compression, respectively. We note that for values of $K = 1$, 5, and 10 $\langle R_{g,z} \rangle^2$ (which corresponds roughly to brush thickness) varies by no more than 5%, and thus brush thickness shows little dependence on K over the range 1−10. We conclude that for our systems nonuniform compression does not affect brush formation. However, nonuniform compression has been shown to play a role in MAMs formation by experiment.[14] One might posit that this disparity stems from our use of periodic boundary conditions (PBCs) which mimic an infinite surface in both directions, regardless of the dimensions of the simulation box in that direction. PBCs introduce an artificial periodicity in the x- and y-directions which might cause compression effects to propagate faster than in experimental systems. Certainly we could turn off PBC to study nonuniform compression; but by doing so, we lose one computational advantage at our disposal, and this was not the main focus of this work.

IV. Comparison with SCF Theory and Previous Results

As stated earlier, SCF theory was used to show that the density profile for polymer brushes of short chains could be described with a parabolic equation; we offer here an alternative form of eq 3:

$$\rho(z) = \rho_0 - \alpha z^2 \tag{19}$$

with $\rho_0 = C_1 \rho_a^{2/3}$ and $\alpha = C_2 N^{-2}$ (C_1 and C_2 are two adjustable parameters). Accordingly, density profile data were collected during slow compression. We plotted the normalized density profiles for 20-mers, 50-mers, and 100-mers at several densities (approximately 0.03, 0.10, 0.20, and 0.50 monomers/area). Portions of the curves of the form $A - Bz^2$ (eq 19) were fit to these profiles (Figures 11–13), and C_1 and C_2 were extracted. The goodness of the fit is primarily a function of surface density, ρ_a, and is independent of chain length: at low surface density, ρ_a, parabolic form was applicable to a majority of the chain monomers; conversely, at high surface density, parabolic form was applicable only for the chain end farthest from the tethering surface. Deviations from parabolic form are apparent in the plots. Figure 11 shows the density profile for 20-mers. The density profile $\rho(z)$ fluctuates significantly near the surface for the highest density (0.499 monomers/area); monomer units near the

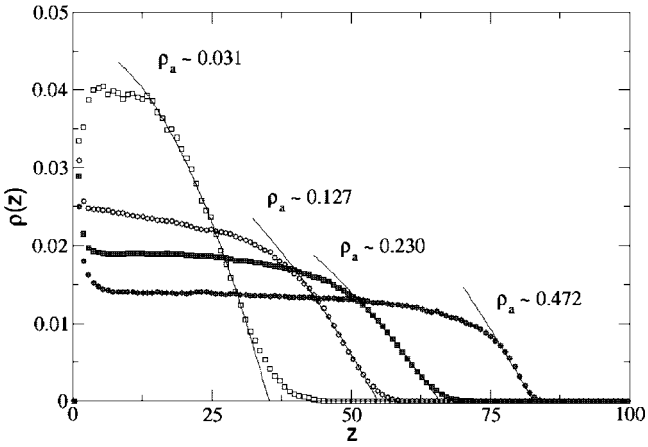

Figure 13. Density profile $\rho(z)$ vs z showing C_1/C_2 fit of eq 19 for 100-mers at various values of ρ_a.

Table 2. Maximum Brush Height, h_{max}, Fit Variables, C_1 and C_2, and Average Brush Height, $\langle z \rangle$, for Chains of Length, N, and Surface Density, ρ_a; Also Shown for Comparison Are Murat and Grest (MG) Data

		h_{max}		C_1	C_2		
N	ρ_a	data	MG	$\rho_0/\rho_a^{2/3}$	αN^2	SQRT(C_1/C_2)	$h_{max}/\langle z \rangle$
20	0.032	8.3	7.9	2.183	1.280	1.31	2.04
20	0.102	11.2	10.7	0.733	0.508	1.20	2.31
20	0.195	13.2		0.476	0.368	1.14	2.28
20	0.499	16.9		0.326	0.288	1.06	2.16
50	0.031	18.2	18.0	0.058	0.043	1.16	2.28
50	0.100	25.3	25.1	0.016	0.014	1.09	2.37
50	0.200	30.6	30.7	0.009	0.008	1.05	2.29
50	0.475	40.9		0.004	0.003	1.05	2.21
100	0.031	35.3	33.9	0.466	0.370	1.12	2.39
100	0.127	54.8		0.142	0.120	1.09	2.40
100	0.230	65.9		0.088	0.076	1.08	2.35
100	0.472	82.7		0.086	0.076	1.06	2.20

surface are being forced to take positions in z of discrete multiples of σ. By comparison, lower surface density ($\rho_a = 0.032$) shows a better parabolic fit. Figure 12 shows the density profile for 50-mers; we see that for surface densities $\rho_a > 0.200$ there exists a significant range where $\rho(z)$ is nearly independent of z, corroborating scaling theory by Alexander.[16,17] This trend is further magnified when one looks at even longer chains. Figure 13 shows the density profile for 100-mers, and we see that at surface densities near 0.500, $\rho(z)$ is linear with respect to z, and there exists only a small portion of the chain (about 1/3) which fits the parabolic function. In other words, the parabolic form for the density profile fits the data well only for low surface density. Also, as chain length increases, the deviation from parabolic form is further magnified; this is in good agreement with SCF theory from section I.

Our values for C_1 and C_2 are reported in Table 2. From this, one can extract the maximum height of the brush, $h_{max} = (\rho_0/\alpha)^{1/2}$. Our values of h_{max} show good agreement with the values from Murat and Grest.[38] Expanding $h_{max} = (\rho_0/\alpha)^{1/2}$, we get $h_{max} = (C_1\rho_a^{2/3}N^2/C_2)^{1/2} = N\rho_a^{1/3}(C_1/C_2)^{1/2}$. From Table 2, we see that as chain length (N) or surface density (ρ_a) increases, $(C_1/C_2)^{1/2}$ trends toward unity. This fits well with Alexander's scaling theory (good solvent or hard sphere) and SCF theory (long chains), which says $h \sim N\rho_a^{1/3}$ (eq 2). Also, we have calculated $h_{max}/\langle z \rangle$, where $\langle z \rangle$ is the average brush height defined by

$$\langle z \rangle = \int \rho(z) z \, dz / \int \rho(z) \, dz \tag{20}$$

We see that $h_{max} \sim 2.0-2.3$ times $\langle z \rangle$ for all cases. This corresponds as well with data in ref 35.

Using the value of h_{max} from above, we also fit the SCF model for the end-monomer density profile (eqs 4 and 5) to our normalized $\rho_E(z)$ plots. For the case of 100-mer systems, the values for C_3 and C_4 fell in the range 0.7−1.0, with eq 4 valid at surface densities $\rho_a < 0.1$ and eq 5 valid for $\rho_a > 0.1$. For 50-mers, C_3 and C_4 were 0.3−0.5, again with eq 4 applicable to $\rho_a < 0.1$ and eq 5 valid for $\rho_a > 0.1$.

In general, deviations of our results from SCF theory or data collected by Murat and Grest are minimal. These comparisons included monolayer thickness, density profiles, and end-monomer profiles. While SCF theory implies equilibrium at a constant surface density and work by Murat and Grest presented data from equilibrated systems at constant surface densities, we have shown that compression of a monolayer in good solvent does not result in deviation from theory or prior simulation results. From this, we conclude that the change in the surface density inherent in the mechanically assembled monolayer process does not conflict with current polymer brush theory and that the model and simulation process presented herein capture the general mechanism underlying the MAMs formation process. This finding acts as a basis for future investigation into systems of poorer solvent quality and more realistic polymers such as alkanes.

V. Conclusions

We have performed discontinuous molecular dynamics simulation of compressed polymer brushes in good solvent, thereby mimicking the mechanically assembled monolayer process. Brush height, monomer density profiles, and end-monomer density profiles corresponded well to theoretical predictions from Alexander and DeGennes and self-consistent-field theory as well as to previous simulations performed by Murat and Grest on tethered polymer systems. Brush thickness and order were measured as a function of surface density. We found that thick uniform brushes required either long chains or high surface density. It was shown that one advantage of long-chained systems (say, $N \geq 50$) compared to shorter-chained systems is that complete surface coverage could be accomplished at a lower surface density; thus, MAMs for long-chain systems require less initial mechanical manipulation compared to short-chain systems to form effective barriers. As surface density increased, polymers began to align in the z-direction (away from the tethering surface); on the other hand, there was no visible x- and/or y-direction alignment, suggesting we saw no crystal formation in this good solvent. Also, at high surface density, end-monomer units tended to move far from the tethering surface. This is crucial in "good" MAMs formation since end-monomer units are typically tailored for specific purposes in the subsequent brush environment. Next, we studied the effect of surface compression rate on the brush thickness, especially in the region where compressions occurred more frequently than the brush equilibration rate. It was noted that in general slower compression rates represent a quasi-equilibrium state that matches equilibrium data closely; faster compression rates increased the discrepancy between our brush heights and values from previous simulation results collected at equilibrium. More specifically, quick compression rates for short-chained systems led to high brush thickness values (relative to equilibrium data) due to lack of equilibration time while quick compression for longer chains led to polymer entanglement problems in the brush. In general, we propose that to minimize deleterious effects to brush thickness and structure, experimentalists should reduce MAM formation rate as homopolymer length increases. Similarly, deleterious effects of compression rate on brush height were seen when hysteresis was investigated; slow relaxation of the surface resulted in brush thickness values that more closely matched compression data than faster relaxation. Last, we have

shown that there is little effect on brush formation by nonuniform compression, in disagreement with experimental findings.

Acknowledgment. This work was supported by the Director, Office of Energy Research, Office of Basic Sciences, Chemical Science Division of the U.S. Department of Energy under Grant DE-FG05-91ER14181. Jan Genzer thanks National Science Foundation and the Office of Naval Research for financial support through Grants CTS-0403535 and N00014-07-0253, respectively.

References and Notes

(1) Adamson, A. W. In *Physical Chemistry of Surfaces*, 4th ed.; Wiley-Interscience: New York, 1984.
(2) Murray, R. W. Chemically Modified Electrodes. *Acc. Chem. Res.* **1980**, *13* (5), 135–141.
(3) Soriaga, M. P.; Hubbard, A. T. Determination of the Orientation of Aromatic-Molecules on Platinum-Electrodes. *J. Am. Chem. Soc.* **1982**, *104* (14), 3937–3945.
(4) Kuhn, H.; Mobius, D. In *Techniques of Chemistry*; Wiley, New York, 1972; p 577.
(5) Knoll, W.; Philpott, M. R.; Golden, W. G. Surface Infrared And Surface Enhanced Raman Vibrational-Spectra Of Monolayer Assemblies In Contact With Rough Metal-Surfaces. *J. Chem. Phys.* **1982**, *77* (1), 219–225.
(6) Whitten, D. G. Photo-Chemical Reactions In Organized Monolayer Assemblies. *Angew. Chem., Int. Ed. Engl.* **1979**, *18* (6), 440–450.
(7) Polymeropoulos, E. E.; Sagiv, J. Electrical-Conduction Through Adsorbed Monolayers. *J. Chem. Phys.* **1978**, *69* (5), 1836–1847.
(8) Richard, M. A.; Deutch, J.; Whitesides, G. M. Hydrogenation Of Oriented Monolayers Of Omega-Unsaturated Fatty-Acids Supported On Platinum. *J. Am. Chem. Soc.* **1978**, *100* (21), 6613–6625.
(9) Waldbillig, R. C.; Robertson, J. D.; McIntosh, T. J. Images Of Divalent-Cations In Unstained Symmetric And Asymmetric Lipid Bilayers. *Biochim. Phiophys. Acta* **1976**, *448* (1), 1–14.
(10) Nuzzo, R. G.; Allara, D. L. Adsorption Of Bifunctional Organic Disulfides On Gold Surfaces. *J. Am. Chem. Soc.* **1983**, *105* (13), 4481–4483.
(11) Efimenko, K.; Genzer, J. Tuning The Surface Properties Of Elastomers Using Hydrocarbon-Based Mechanically Assembled Monolayers. *Mater. Res. Soc. Symp. Proc.* **2002**, *705*, DD10.3.1DD10.3.6.
(12) Tomlinson, M. R.; Wu, T.; Efimenko, K.; Genzer, J. Gradient Polymer Brushes: Preparation And Applications. *Polym. Prepr.* **2003**, *44* (1), 468.
(13) Genzer, J.; Efimenko, K. Creating Long-Lived Superhydrophobic Polymer Surfaces Through Mechanically Assembled Monolayers. *Science* **2000**, *290* (5499), 2130–2133.
(14) Wu, T.; Efimenko, K.; Genzer, J. Preparing High-Density Polymer Brushes by Mechanically Assisted Polymer Assembly (MAPA). *Macromolecules* **2001**, *34*, 684–686.
(15) Genzer, J.; Fisher, D. A.; Efimenko, K. Fabricating Two-Dimensional Molecular Gradients via Asymmetric Deformation of Uniformly-Coated Elastomer Sheets. *Adv. Mater.* **2003**, *15*, 1545–1547.
(16) Alexander, S. Adsorption Of Chain Molecules With A Polar Head A-Scaling Description. *J. Phys. (Paris)* **1977**, *38* (8), 983–987.
(17) de Gennes, P.-G. Conformations Of Polymers Attached To An Interface. *Macromolecules* **1980**, *13* (5), 1069–1075.
(18) de Gennes, P.-G. *Scaling Concepts in Polymer Physics*; Cornell University Press: Ithaca, NY, 1979.
(19) Binder, K. *Monte Carlo and Molecular Dynamics Simulations in Polymer Science*; Oxford University Press: New York, 1995.
(20) Skvortsov, A. M.; Pavlushkov, I. V.; Gorbunov, A. A.; et al. *Polym. Sci. USSR* **1988**, *30*, 487.
(21) Milner, S. T.; Witten, T. A.; Cates, M. E. Theory Of The Grafted Polymer Brush. *Macromolecules* **1988**, *21* (8), 2610–2619.
(22) Milner, S. T.; Wang, Z. G.; Witten, T. A. End-Confined Polymers—Corrections To The Newtonian Limit. *Macromolecules* **1989**, *22* (1), 489–490.
(23) Zhulina, E. B.; Borisov, O. V.; Pryamitsyn, V. A. Theory Of Steric Stabilization Of Colloid Dispersions By Grafted Polymers. *J. Colloid Interface Sci.* **1990**, *137* (2), 495–511.
(24) Auroy, P.; Auvray, L.; Leger, L. The Study Of Grafted Polymer Layers By Neutron-Scattering. *J. Phys.: Condens. Matter* **1990**, *2*, SA317–SA321.
(25) Cosgrove, T. Volume-Fraction Profiles Of Adsorbed Polymers. *J. Chem. Soc., Faraday Trans.* **1990**, *86* (9), 1323–1332.
(26) Auroy, P.; Auvray, L. Collapse-Stretching Transition For Polymer Brushes—Preferential Solvation. *Macromolecules* **1992**, *25* (16), 4134–4141.
(27) Auroy, P.; Auvray, L. About The Sensitivity Of The Small-Angle Neutron-Scattering Technique In The Determination Of A Polymer Interfacial Density Profile. *J. Phys. II* **1993**, *3* (2), 227–243.
(28) Semenov, A. N. Contribution To The Theory Of Microphase Layering In Block-Copolymer Melts. *Zh. Eksp. Teor. Fiz.* **1985**, *88* (4), 1242–1256.
(29) Alder, B. J.; Wainwright, T. E. Studies In Molecular Dynamics. *J. Chem. Phys.* **1959**, *31* (2), 459–466.
(30) Allen, M. P.; Tildesley, D. J. *Computer Simulation of Liquids*; Clarendon Press: Oxford, 1987.
(31) Haile, J. M. *Molecular Dynamics Simulation*; Wiley: New York, 1992.
(32) Smith, S. W.; Hall, C. K.; Freeman, B. D. Molecular Dynamics For Polymeric Fluids Using Discontinuous Potentials. *J. Comput. Phys.* **1997**, *134* (1), 16–30.
(33) Rapaport, D. C. Molecular-Dynamics Simulation Of Polymer-Chains With Excluded Volume. *J. Phys. A: Math. Gen.* **1978**, *11* (8), L213–L217.
(34) Rapaport, D. C. Molecular-Dynamics Study Of A Polymer-Chain In Solution. *J. Chem. Phys.* **1979**, *71* (8), 3299–3303.
(35) Bellemans, A.; Orban, J.; Van Belle, D. Molecular-Dynamics Of Rigid And Non-Rigid Necklaces Of Hard Disks. *Mol. Phys.* **1980**, *39* (3), 781–782.
(36) Andersen, H. C. Molecular-Dynamics Simulations At Constant Pressure And-Or Temperature. *J. Chem. Phys.* **1980**, *72* (4), 2384–2393.
(37) Kenkare, N. R.; Smith, S. W.; Hall, C. K. Discontinuous Molecular Dynamics Studies Of End-Linked Polymer Networks. *Macromolecules* **1998**, *31* (17), 5861–5879.
(38) Murat, M.; Grest, G. S. Structure Of A Grafted Polymer Brush: A Molecular Dynamics Simulation. *Macromolecules* **1989**, *22* (10), 4054–4059.
(39) Carignano, M. A.; Szleifer, I. Statistical Thermodynamic Theory Of Grafted Polymeric Layers. *J. Chem. Phys.* **1993**, *98* (6), 5006–5018.
(40) Szleifer, I.; Carignano, M. A. Tethered Polymer Layers. *Adv. Chem. Phys.* **1996**, *94*, 165–260.

MA8003218